01 Jan 2024

The Hydration, Microstructure, And Mechanical Properties Of Vaterite Calcined Clay Cement (VC^3)

Yaqiang Li

Yue Li

Hongyan Ma
Missouri University of Science and Technology, mahon@mst.edu

Jiaqi Li

Recommended Citation

Y. Li et al., "The Hydration, Microstructure, And Mechanical Properties Of Vaterite Calcined Clay Cement (VC^3)," *Cement and Concrete Research*, vol. 175, article no. 107374, Elsevier, Jan 2024.
The definitive version is available at https://doi.org/10.1016/j.cemconres.2023.107374

Cement and Concrete Research 175 (2024) 107374

Contents lists available at ScienceDirect

Cement and Concrete Research

journal homepage: www.elsevier.com/locate/cemconres

The hydration, microstructure, and mechanical properties of vaterite calcined clay cement (VC^3)

Yaqiang Li [a,*], Yue Li [b,*], Hongyan Ma [c], Jiaqi Li [d,*]

[a] Department of Civil Engineering, Beijing Forestry University, Beijing 100083, China
[b] The Key Laboratory of Urban Security and Disaster Engineering, MOE, Beijing University of Technology, Beijing 100124, China
[c] Missouri University of Science & Technology, Department of Civil Architectural & Environmental Engineering, Rolla, MO 65409, United States
[d] Atmospheric, Earth, and Energy Division, Lawrence Livermore National Laboratory, Livermore 94550, United States

ARTICLE INFO

Keywords:
Carbon utilization
Carbon storage
CCUS
Bio-inspired
Low-CO_2 cement

ABSTRACT

Limestone (calcite) calcined clay cement (LC^3) is a promising low-CO_2 binder, but the low activity of calcite cannot compensate the reduction in clinker factor, resulting in low one-day strength and limiting its broad applications. As recent carbon capture and utilization technologies allow scalable production of vaterite, a more reactive $CaCO_3$ polymorph, we overcome the challenge by introducing vaterite calcined clay cement (VC^3), inspired by the vaterite-calcite phase change. In the present study, VC^3 exhibits higher compressive strengths and faster hydration than LC^3. Compared to hydrated LC^3, hydrated VC^3 exhibits increased amount of hemi- and mono-carboaluminate formation and decreased amount of strätlingite formation. With gypsum adjustment, the 1-day strength of VC^3 is higher than that of pure cement reference. VC^3, a low-CO_2 binder, presents great potential as a host of the metastable $CaCO_3$ for carbon storage and utilization and as an enabler of carbon capture at gigaton scales.

1. Introduction

Portland cement is the most versatile binder in construction, with current production of over 4 Gt/year and a projected increase in demand by 50% [1]. The massive cement production accounts for ~8% of global anthropogenic CO_2 emissions [2]. As the second largest commodity after freshwater, the decarbonization of cement is of great interest but great challenges as well. Gigaton-scale decarbonization by alternative or blended low-carbon cement is handicapped by economic viability, technical feasibility, and scalability (e.g., raw materials distribution) [3].

Most modern cement kilns are at or close to the maximum thermal efficiency [4]; thus, decarbonization strategies have focused on exploring materials alternative or supplementary to cement. The partial cement clinker replacement by supplementary cementitious materials (SCMs, e.g., coal fly ash) is a mature cement decarbonization strategy [5]. However, due to the global energy transition, in recent years, byproduct SCMs from other industries (e.g., fly ash from coal power plants and granulated blast furnace slag from iron manufacturing) could not meet the massive cement demand [6]. With the high natural reservoir capacity of limestone (calcite), limestone calcined clay cement (LC^3) has been widely validated as a scalable, low-cost solution to cement decarbonization at a clinker content of up to 50% [7,8]. Both limestone and clay are locally available and massively sourced at low costs. LC^3 with 50% clinker replacement can achieve equivalent strengths to ordinary Portland cement by 3 days [9], exhibiting higher late-age mechanical properties due to refined microstructure by reactions between clinker / hydrates, limestone, and calcined clay (mainly metakaolin) [10]. Besides calcium aluminosilicate hydrate (C-A-S-H), other major reaction products (i.e., hemicarboaluminate, monocarboaluminate, and strätlingite) also play important roles in the enhanced durability of LC^3 [11]. Requiring no special handling or training, the LC^3 technology has been readily deployable at scale [12].

Despite many advantages and industrial interests [13], LC^3 presents unignorable limitations: 1) low early-age strengths (e.g., at 1 day) [14]; 2) complex rheology (e.g., poor flowability) [15]; and 3) production slowdown due to enhanced needs for grinding specific components of LC^3. While inter-grinding clinker, gypsum, calcined clay, and limestone using mills does not reduce the productivity of blended cement, the particle size distribution of each component of LC^3 is difficult to optimize, thus affecting productivity. Thus, the common strategy, e.g., in the U.S. markets, is instead inter-blending where Portland cement, calcined

* Corresponding authors.
E-mail addresses: liyaqiang@bjfu.edu.cn (Y. Li), liyue@bjut.edu.cn (Y. Li), li88@llnl.gov (J. Li).

https://doi.org/10.1016/j.cemconres.2023.107374
Received 7 February 2023; Received in revised form 2 October 2023; Accepted 5 November 2023
Available online 8 November 2023

clay, and limestone are individually ground to the required fineness and blended together [16], compromising the production rate.

The low 1-day strength of LC^3 may be mitigated by chloride-based [17] or calcium silicate hydrate (C-S-H) seed-based accelerators [18]. However, using such accelerators limits the use of LC^3 concrete to non-reinforced applications or at low water-to-cement ratios [17,19]. The abovementioned limitations may be resolved simultaneously with the new ternary Portland cement system – vaterite calcined clay cement (VC^3), in which the limestone powders of LC^3 are replaced by vaterite, a metastable $CaCO_3$ polymorph with a higher reactivity in Ca-rich cementitious systems, compared to calcite [20]. Additionally, the spherical nature of vaterite particles mitigates the flowability issue associated with LC^3. Recent advances in the deployment of climate technology (e.g., by Calera and Fortera) allow low-cost production of vaterite at scale with co-benefits of air CO_2 capture or point source carbon capture [21]. The global warming potential of vaterite production through carbon storage depends on the carbon footprint of energy use (e.g., renewable electricity), CO_2 capture efficiency, raw materials, and type of processes. Via the "climate tech" pioneers, the embodied carbon of vaterite production could be down to 0.3 kg CO_2 per kg of vaterite produced, while stoichiometrically, 1 kg of vaterite can store 0.44 kg of CO_2. Thus, vaterite can be potentially produced at an overall "negative" carbon embodiment (i.e., −0.14 kg CO_2/kg vaterite).

A proof-of-concept study is needed for the potential outperformance of VC^3 over LC^3. Although VC^3 is similar to LC^3 at first glance, metastable vaterite may alter the chemistry and microstructure of the ternary blended cement system and late-age strengths (e.g., at 28 days). The following intriguing questions remain unknown: 1) does the more reactive $CaCO_3$ polymorph increase the formation of hemi- or monocarboaluminate? 2) does the competition for aluminum in metakaolin limit the formation of strätlingite? and 3) does vaterite lead to higher 28-day strengths of VC^3 relative to LC^3?

In this study, we investigated the properties of vaterite and metakaolin-blended Portland cement as the proof-of-concept for the proposed VC^3 at a clinker content of ~50%. While applying comparable particle sizes of $CaCO_3$, we examined the mechanical properties, hydration, and microstructure of our VC^3 system and compared with those of the classic LC^3 system. To validate improved early-age performance, the hydrated VC^3 and LC^3 (the same metakaolin-to-$CaCO_3$ mass ratio of 2) at 1-day age were characterized using X-ray diffraction (XRD), scanning electron microscopy (SEM), isothermal calorimetry, and thermogravimetric analysis (TGA). The compressive strengths of VC^3 were optimized by sulfation adjustment and measured up to 28 days.

The present work unveils the chemistry and materials properties of the new low-CO_2 ternary blended system, VC^3, and motivates continued studies on VC^3 durability and rheology, inspires the development of vaterite-rich blended cement, and provides implications for gigaton-scale enablers of air CO_2 capture and storage as well as point source carbon capture and storage.

2. Materials and methods

2.1. Materials

Type I ordinary Portland cement (OPC) was used in this study. Metakaolin with >96% purity was obtained from BASF Metamax. Vaterite was synthesized following the protocol in [22,23]. Briefly, vaterite was prepared by mixing $CaCl_2$ and Na_2CO_3 aqueous solutions at a molar ratio of 1:1 at 25 °C, followed by 1 min of centrifuging at 5000 rpm. The precipitate was rinsed with ethanol and dried at 50 °C for 12 h. Calcite was prepared by ball-milling limestone powder for 30 min. Details of the chemical compositions and physical properties of raw materials are given in Table 1, Table 2, and Fig. 1. Calcite (>99% purity) shows slightly smaller D50 compared to vaterite (>95% purity) but a broader range of particle size distribution. Fig. 2 shows the morphology of calcite and vaterite. The vaterite synthesized in this study is morphologically similar to that prepared from carbon capture [21]. A polycarboxylate ether (PCE)-based superplasticizer (powder, SIKA) was used to ensure optimal workability for selected mix proportions.

Table 1
Chemical compositions of ordinary Portland cement and metakaolin used in this study.

Oxides	OPC (%)	Metakaolin (%)	Crystalline phases of OPC	Content (%)
CaO	67.36	0.02	C_3S	61.28
SiO_2	19.04	51.96	C_2S	18.43
Fe_2O_3	3.74	0.46	C_3A	5.85
SO_3	3.22	0.06	C_4AF	7.94
Al_2O_3	3.16	44.34	Gypsum ($C\$H_2$)	3.65
MgO	1.67	0.00	Dolomite	1.28
K_2O	0.66	0.11	Periclase	0.64
TiO_2	0.60	2.65	Quartz	0.42
Na_2O	0.29	0.25	Calcite	0.51
MnO	0.07	0.00	/	/
LOI	0.19	0.15	/	/

Note: LOI = Loss on ignition; Cement notation: C = CaO, S = SiO_2, A = Al_2O_3, F = Fe_2O_3, $ = SO_3, H = H_2O.

Table 2
Particle size distribution, specific surface area, and specific gravity of raw materials.

Materials	D10 (μm)	D50 (μm)	D90 (μm)	Specific surface area (m^2/g)	Density (g/cm^3)
Cement	2.41	16.95	44.42	1.27	3.1
Vaterite	1.08	5.92	10.52	65.72	2.54
Calcite	0.75	5.04	35.95	2.78	2.71
Metakaolin	0.93	3.75	13.13	21.62	2.23
Gypsum	18.65	64.60	140.22	0.24	2.32

The mix proportions and the nomenclature used in this study are given in Table 3. Coupled substitutions of metakaolin and calcite or vaterite were mixed at the mass ratio 2:1.

2.2. Methods

For preparing blended cement pastes, the powders were first dry-mixed at 25 °C for 1 min at 150 rpm, followed by the mixing with water and superplasticizer for 3 min at 300 rpm. All pastes were cast at a water-to-binder (w/b) ratio of 0.5 at 25 °C.

The flowability (mini-slump) test follows the protocol in [24]. The test was conducted by placing a moistened cone on a moistened flat plate. The dimensions of the top and bottom rims and the height of the moistened cone are 36 mm, 60 mm, and 60 mm, respectively. Each paste was poured into the cone immediately after mixing and compacted using a moistened rod. The cone was lifted vertically, and the diameter of the spread was measured at 30 s.

Setting time measurement of pastes was conducted according to the Vicat needle test per ASTM C191.

Reaction heat of pastes were measured at 25 °C using an 8-channel isothermal conduction calorimeter (TAM Air). Four grams of fresh paste at w/b of 0.5 were loaded.

For compressive strength measurement, the pastes were cast into cubic molds with side length of 20 mm, then sealed, and cured at 25 °C until testing. For each mix proportion, at least three cubes were measured at each curing age.

The hydration of paste samples was stopped at designated ages by immersion of 5 mm-thick slices in pure isopropanol for at least three days. The samples were vacuum-dried at 40 °C for at least two days to remove isopropanol, then placed in vacuum desiccator until testing to prevent carbonation.

X-ray diffraction patterns were collected for the samples using a Rigaku Ultima IV diffractometer operating at 40 kV with 40 mA using a copper target. 15% corundum was blended into powdered hardened

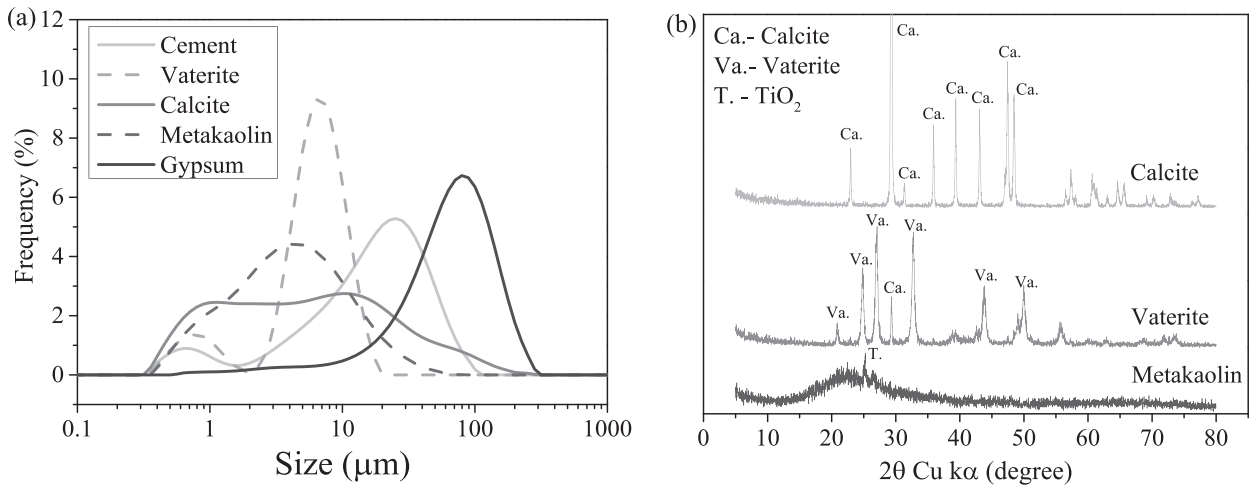

Fig. 1. Particle size distribution and diffraction patterns of raw materials. (a) Particle size distribution; (b) XRD patterns.

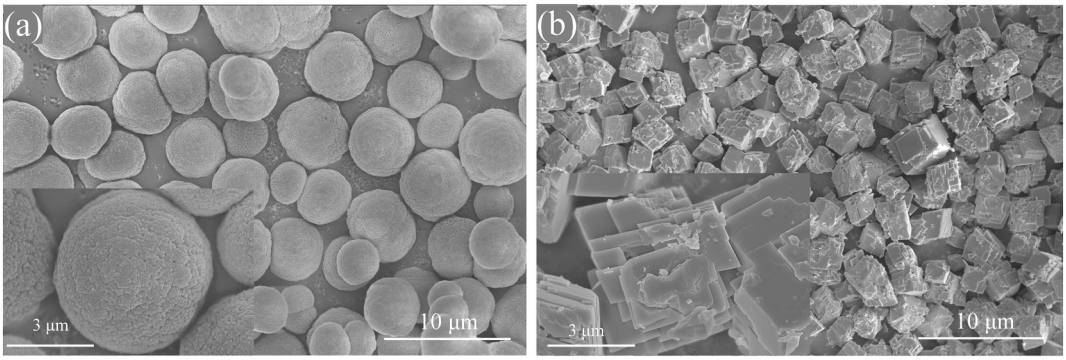

Fig. 2. SEM micrographs of vaterite and calcite showing distinct morphologies. (a) Vaterite; (b) Calcite.

Table 3
Mix proportions used in this study.

	OPC (g)	Calcite (g)	Vaterite (g)	Metakaolin (g)	Gypsum (g)	Water (g)	PCE (g)
OPC	100	–	–	–	–	50	–
PLC	85	15	–	–	–	50	–
PVC	85		15	–	–	50	–
LC^3	55	15	–	30	–	50	0.2
VC^3	55	–	15	30	–	50	0.2
VC^3–1.5C$	54.175	–	14.775	29.55	1.3	50	0.2
VC^3–3.0C$	53.35	–	14.55	29.1	3	50	0.2

pastes and ground together for quantitative X-ray diffraction (QXRD). The major phases were quantified by the reference intensity ratio (RIR) method. All scans were taken from 5° to 75° at a scan rate of 2°/min.

Dried powders were measured using thermogravimetric analysis (TGA) from 30 °C to 1000 °C at a heating rate of 10 °C/min under N_2 protection.

Mercury intrusion porosimetry (MIP) was used to probe the pore structure of the pastes at 1 day. The pore size distribution of LC^3 and VC^3 pastes at 1 day was collected from an AutoPore Iv 9510 porosimeter at a maximum pressure of 414 MPa.

Fractured surfaces of hardened pastes after platinum sputtering were imaged using scanning electron microscopy (NovananoSEM, FEI) at 10 keV under high vacuum. The determination of C-(A)-S-H composition was obtained by Energy Dispersive X-Ray Spectroscopy (EDS) on polished samples. The hardened paste was vacuum impregnated in the epoxy resin (EpoKwick, Buehler) and polished with silicon carbide (SiC) papers (#1200, #2500, and #5000) for 20 min per level of grit.

3. Results and analysis

3.1. Flowability and setting time

With 15% vaterite (D50 = 5.917 μm) and calcite (D50 = 5.042 μm) particles, the flowability of fresh Porltand limestone cement (PLC) and Porltand vaterite cement (PVC) pastes was ~0.8 cm lower than that of OPC (Fig. 3a) due to the finer particle sizes of $CaCO_3$ than that of OPC (D50 = 16.95 μm). Unlike fly ash microspheres, vaterite microspheres did not promote paste fluidity [25], explained by the high-water demand of vaterite due to the rough surface texture of vaterite spheres, the porous structure, and consequently high specific surface area, which was 65.7 m^2/g for vaterite, compared to 1.3 m^2/g for OPC. Compared with PLC, PVC is slightly more flowable due to the presence of vaterite, benefiting from the spherical particles and a larger D50 relative to calcite while partially compromised by the high specific surface area. The flowability of fresh ternary blended cement pastes, LC^3 and VC^3,

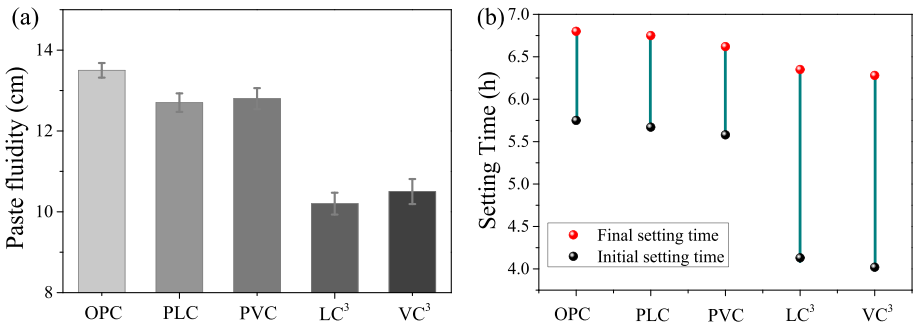

Fig. 3. Workability. (a) Flowability of pastes; (b) Initial and final setting time of pastes.

with the presence of 0.2% PCE, was ~2 cm lower than that of OPC. It is generally agreed that the high-water demand and flocculation induced by the high specific surface area and layered nanostructure of metakaolin results in the poor flowability of LC^3 [15,26]. The flowability of VC^3 was ~0.5 cm higher than that of LC^3 due to the presence of vaterite microspheres. For the comparison between PLC and PVC, the spherical morphology of vaterite helped to improve the fluidity. However, the larger specific surface area of vaterite (65.7 m^2/g) than calcite (2.78 m^2/g) leads to the negative effect of high-water demand on flowability compared with OPC. Under the combined effects, vaterite-blended cements showed higher flowability than that of calcite-blended cements. Nevertheless, because the difference in flowability of calcite-blended cements and vaterite-blended cements is insignificant, within the error range, further research is needed for the rheological properties of vaterite-blended cements.

The initial setting times of PLC and PVC were ~7 min and ~10 min earlier than that of OPC (Fig. 3b), respectively, as explained by the nucleation effect of $CaCO_3$ [27]. The initial setting time of PVC was ~5 min earlier than that of PLC due to the higher degree of hydration promotion caused by vaterite than by calcite. The final setting times of PLC and OPC were comparable because the dilution effect of calcite is compensated by the reaction between calcite and clinker [28–30]. The final setting time of PVC was earlier than that of OPC and PLC due to the higher solubility and reactivity of vaterite. The initial and final setting times of LC^3 and VC^3 were consistently ~1 h earlier than those of OPC due to accelerated cement hydration by the fine metakaolin grains [31]. Compared with LC^3, the faster initial and final setting of VC^3 may additionally be attributed to the higher specific surface area and reactivity of vaterite. More details of cement hydration will be explained in later sections.

3.2. Compressive strengths

Fig. 4 shows that PLC and PVC had lower strength than OPC at the same curing ages due to the lower clinker content in the binary cement systems, while PVC showed about 1–4 MPa higher strengths than PLC at all ages. The 1-day strengths of LC^3 and VC^3 were 44% and 25%, respectively, lower than that of OPC, while the later-age strengths of the ternary cement systems were ~ 8–50% higher than those of OPC. The low 1-day strength of samples without gypsum adjustment is consistent with previous findings, in which LC^3 gained ~40–60% 1-day strength of OPC depending on the particle size and purity of calcite and metakaolin [10,14,32]. Calcite shows slightly smaller D50 compared to vaterite but a broader range of particle size distribution. In this case, the strength of VC^3 was 7–15% higher than that of LC^3 at all ages, especially at 1 day. The higher solubility of vaterite ($\log(K_{sp}) = -7.8$, 25 °C) relative to calcite ($\log(K_{sp}) = -8.4$, 25 °C) [33] may favor a higher degree of $CaCO_3$-clinker reaction in PVC and VC^3 compared to PLC and LC^3, resulting in significant improvement in 1-day strength by incorporating vaterite instead of calcite. Additional replacement of cement by 1.5% and 3% gypsum significantly improved the early strength of VC^3. 1-day strengths of VC^3–1.5C$ and VC^3–3.0C$ exceeded that of OPC by 7% and 13%, respectively, corresponding to 32–38% higher 1-day strengths relative to VC^3 without gypsum adjustment. The additional gypsum in VC^3–3.0C$ played an important role in controlling the rate of aluminates reaction and the formation of more ettringite [34], significantly improving the 1-day strengths relative to VC^3.

3.3. X-ray diffraction

The XRD patterns of OPC, PLC, PVC, LC^3, and VC^3 at 1, 7, and 28 days from 5° to 24° (2θ) were shown in Fig. 5. The contents of C_3S, ettringite and carbonate aluminate of samples at 1, 7, and 28 days were

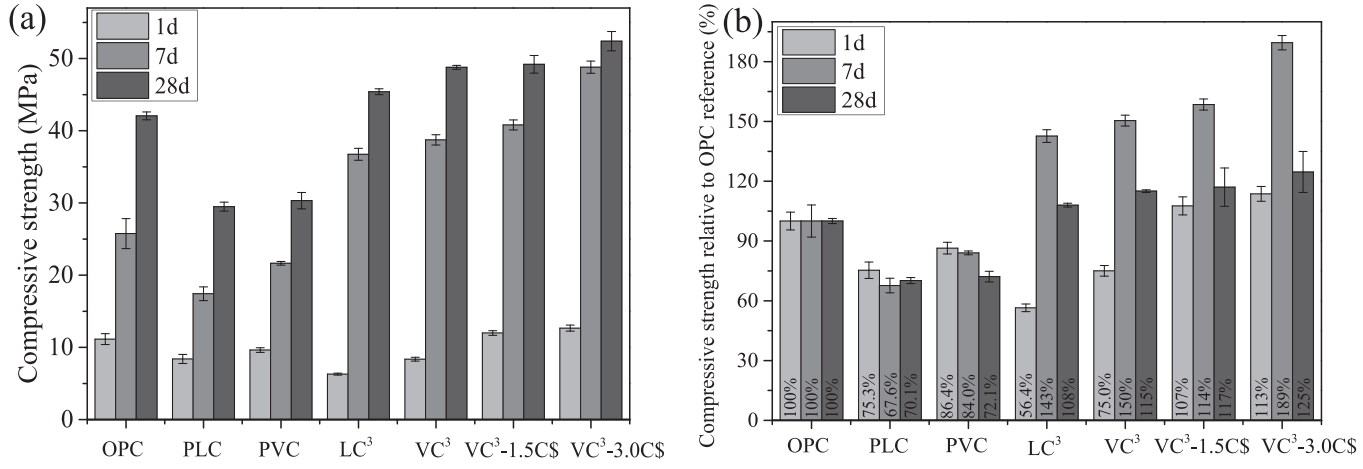

Fig. 4. Compressive strength. (a) Compressive strength of hardened paste; (b) Compressive strength of hardened paste normalized to the strength of OPC.

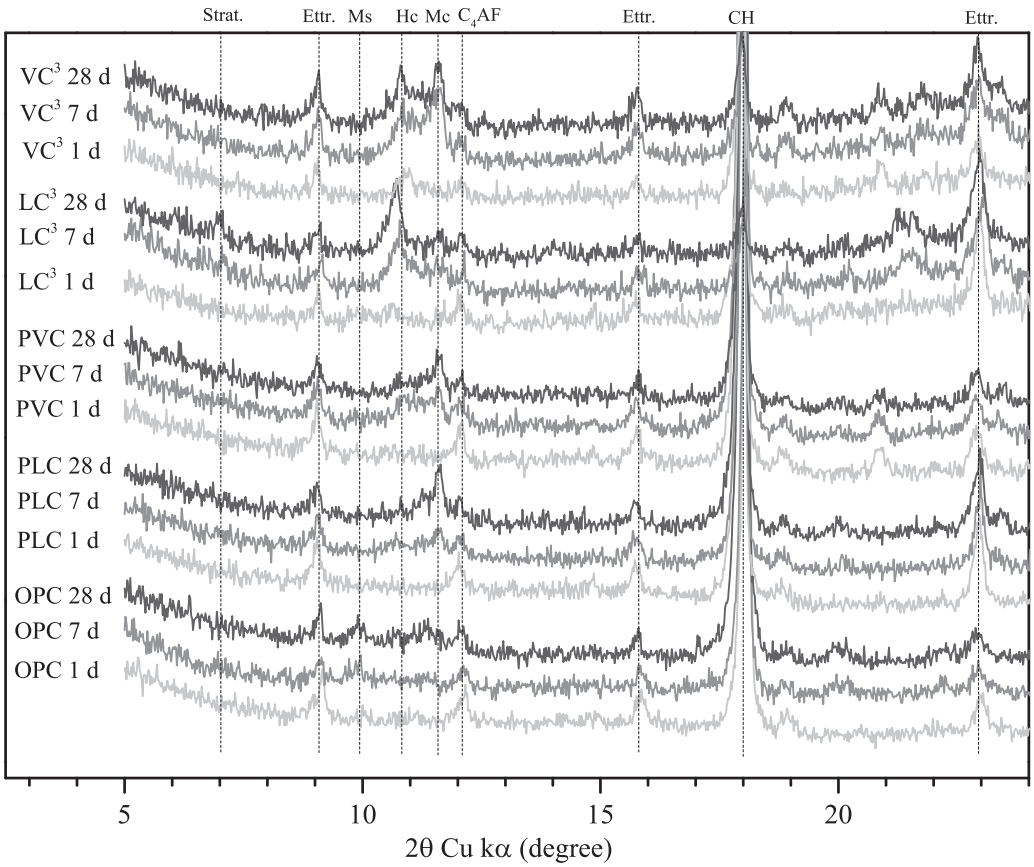

Fig. 5. XRD patterns of OPC, PLC, PVC, LC^3, and VC^3 at 1, 7, and 28 days. The main crystalline phases include strätlingite (Strät.), ettringite (Ettr.), monosulfoaluminate (Ms), hemicarboaluminate (Hc), monocarboaluminate (Mc), portlandite (CH), vaterite (Va.).

determined by QXRD, shown in Fig. s1 and Table s1 (Supplementary Information).

Fig. 5 shows that the major crystalline hydration products of OPC were portlandite, ettringite, and monosulfoaluminate. For PLC, hemicarboaluminate (Hc) and monocarboaluminate (Mc) were observed at 7 days and 28 days, while monosulfoaluminate was not observed at any age. More ettringite was stabilized in PLC than OPC. In the presence of calcite, the formation of carboaluminate hydrates in PLC occurred after sulfate depletion (observed from 7 days) [35], and the predominant formation of Mc due to the low availability of Al in PLC. Similarly, Mc was the primary carboaluminate phase in PVC at 7 days and 28 days.

For LC^3 both Hc and Mc were observed at 7 days and 28 days, along with a decrease in portlandite content. Strätlingite was only observed at 28 days in LC^3. Hc was the dominant form of carboaluminate in LC^3 despite the presence of a large amount of unreacted calcite [36], consistent with previous studies [10]. During cement hydration, metakaolin reacts with portlandite to form C-A-S-H and strätlingite / calcium aluminate hydrate (C_4AH_{13}) phases (Eq.1) [37,38]. However, the reaction of metakaolin is greatly influenced by the anions present in the system. With the presence of sulfate, metakaolin reacts with portlandite and sulfate to form ettringite (Eq.2) [39] and further transforms to monosulfoaluminate after sulfate depletion [37]. With the presence of sulfate and calcite, calcite reacts with metakaolin and portlandite to form Hc (Eq.3) after sulfate depletion [40], while ettringite would be stabilized.

$$AS_2 + (6.2 - 3.1a)CH + (12 - 4.6a)H \rightarrow (2 - a)C_{1.5}A_{0.1}SH_4 + aC_2ASH_8 + (0.8 - 0.9a)C_4AH_{13} \quad (1)$$

$$AS_2 + 5.4CH + 2.4C\$ + 28.2H \rightarrow 0.8C_6A\$_3H_{32} + 2C_{1.5}A_{0.1}SH_4 \quad (2)$$

$$AS_2 + 5.8CH + 0.4C\overline{C} + 11.8H \rightarrow 0.8C_4A\overline{C}_{0.5}H_{12} + 2C_{1.5}A_{0.1}SH_4 \quad (3)$$

$$AS_2 + 5.4CH + 0.8C\overline{C} + 12.2H \rightarrow 0.8C_4A\overline{C}H_{12} + 2C_{1.5}A_{0.1}SH_4 \quad (4)$$

The VC^3 system shows the formation of Hc at 1 day, the formation of Mc at 7 days, and the absence of strätlingite at all ages. VC^3 system maintained a higher content of Mc relative to LC^3 based on QXRD (Table s1, Supplementary Information). Previous studies on LC^3 showed that fine calcite particles also resulted in the formation of Hc at 1 day, which remained as the primary carboaluminate with secondary Mc at the later ages [41]. Compared with calcite (log (K_{sp}) = −8.4, 25 °C), the metastable structure and high solubility of vaterite (log (K_{sp}) = −7.8, 25 °C) facilitate the reaction with aluminum phases. Vaterite can react weakly with Al-rich phases (e.g., C_3A and metakaolin) to form a small amount of Hc before sulfate depletion due to the higher reactivity of vaterite relative to calcite, supported by the observed Hc in VC^3 and the lower ettringite content in VC^3 than LC^3 at 1 day (Table s1, Supplementary Information). The kinetics of Hc formation is faster than Mc, while Mc is thermodynamically more stable [28,42]. Since vaterite is more reactive, its reaction with metakaolin and portlandite seems to favor the formation of Mc rather than Hc, supported by the observed weak peak of Hc phase at 1 day and strong peak of Mc at 7 days and 28 days in VC^3. Previous studies demonstrated that strätlingite can coexist with calcite in silicate cementitious system [43–45]. For LC^3, the reaction between calcite, MK, and CH is weak due to the low reactivity of calcite (Eq.3). The reaction between calcite, MK, and CH reached local equilibrium before 28 days, CH reacted with MK to form strätlingite (Eq.1) at 28 days [46]. In contrast, in VC^3, the highly reactive vaterite participates in the reaction with CH and MK (Eq.3 and Eq.4) to form Hc and Mc.

3.4. Heat of hydration

Fig. 6a shows the 48-h isothermal calorimetry results of fresh pastes, normalized to the content of Portland cement. Two typical exothermic peaks (C_3S hydration at ~7.8 h and C_3A at ~9.7 h) were observed in OPC, PLC, and PVC [47]. Only one peak before 10 h was observed in LC^3 and VC^3 as the exothermic peak of C_3A merged into the peak of C_3S [10], suggesting metakaolin-induced accelerated hydration of C_3A [39]. Both calcite and vaterite increased the slope of the acceleration period. Metakaolin further increased the slope of the acceleration period. The above evidences suggest that calcite, vaterite, and metakaolin provided extra nucleation sites to cement hydration [48]. The induction periods of vaterite-blended cements were shorter than those of calcite-blended cements, consistent with the initial setting time results. Existing literature has shown prolonged induction periods of MK-blended cements than OPC due to the addition of PCE [49]. However, in the present study, the initial setting of MK-blended cements occurred earlier than that of OPC, supported by the significantly greater slope of its hydration acceleration period compared to OPC.

In LC^3, an exothermic peak was detected at 20 h, which was not found in previous studies [50]. As Hc was not observed in our XRD result of LC^3 at 1 day, and exothermic peak of Hc was typically observed during 48–72 h of LC^3 hydration [41], we attribute the exothermic peak at 20 h to ettringite formation from the reaction between portlandite, sulfate, and highly reactive metakaolin (Eq.2). In VC^3, broad exothermic peaks detected between 12 h and 24 h suggest the formation of ettringite and Hc, respectively, supported by XRD results. According to the cumulative heat release curve (Fig. 6b), the order of amount of heat release normalized by cement content is OPC < PLC < PVC < LC^3<VC^3. By comparing PLC versus PVC and LC^3 versus VC^3, vaterite played a critical role in promoting cement hydration in contrast to calcite due to the high reactivity and specific surface area of vaterite. Gypsum adjustments (1.5% and 3%) decreased the slope of the acceleration period of VC^3, suggesting retarded C_3A hydration. The retardation effect was more prominent at the higher gypsum content. From the cumulative heat release curve, gypsum adjustments reduced the heat release of VC^3 before ~12 h. However, with the hydration of aluminates, the heat release of VC^3–1.5C$ exceeded that of VC^3 from 12 h, and the heat release of VC^3–3.0C$ exceeded that of VC^3–1.5C$ from 19 h.

3.5. Thermogravimetric analysis

The smaller area of the thermal decomposition peak of portlandite at ~420 °C in Fig. 7a suggests a significant pozzolanic reaction of metakaolin. A thermal decomposition peak at ~123 °C was observed in VC^3 at 1 day and assigned to Hc [50], consistent with XRD. This peak was also observed in LC^3 and VC^3 at 7 days (Fig. 7b), assigned to Hc and Mc, respectively, based on the XRD results. A thermal decomposition peak of strätlingite at ~196 °C [32] was observed in LC^3 at 28 days (Fig. 7c) but not in VC^3 at 28 days, agreeing with our XRD results.

The content of bound water in hydrated pastes was quantified by the mass loss between 40 °C and 450 °C [51]. The tangent method [52] was used to quantify the portlandite content from the dehydration peak between 350 °C and 450 °C as well as $CaCO_3$ content from the decarbonization peak between 590 °C and 730 °C. The content of bound water and portlandite in each sample was reported in Table 4, normalized to anhydrous OPC content, taking into account the clinker content in blended cement systems. Due to the reaction between metakaolin and $CaCO_3$, the portlandite content in LC^3 and VC^3 systems was comparable, lower than that in OPC. The bound water content in both LC^3 and VC^3 systems was higher than those in OPC, while VC^3 exhibited a slightly higher bound water content than LC^3. The differences suggest that calcite, vaterite, and metakaolin promoted cement hydration, and vaterite presented enhanced effectiveness than calcite.

The portlandite consumption (CH-Consumption) in LC^3 and VC^3 was calculated by taking the portlandite content of OPC as the baseline at the same age considering the clinker content, without considering the accelerated hydration induced by metakaolin and $CaCO_3$, listed in Table 6.

The consumption of metakaolin (MK-Consumption) in LC^3 and VC^3 was calculated based on the portlandite consumption from TGA using Eq. (2), Eq. (3), and Eq. (4). For calculating metakaolin content in LC^3 and VC^3 at 1 day, we assumed that all portlandite was consumed for the formation of ettringite (Eq.2) and Hc (Eq.3), respectively. For calculating metakaolin content at 7 days and 28 days, we assumed all portlandite in LC^3 was consumed for the formation of Hc and Mc (Eq.3 and Eq.4), where the mass ratios of Hc to Mc were determined by QXRD (Table s1). The calculated reaction degrees of metakaolin were listed in Table 6, which showed that the reaction degree of metakaolin in VC^3 was higher than that of LC^3 at the same ages. The reaction degree of MK could be underestimated at early ages, more significantly in VC^3, because the calculation in the present study does not consider the accelerated hydration induced by metakaolin and calcite/vaterite.

The reaction degree (D) of calcite or vaterite in LC^3 and VC^3 can be determined using Eq.5. As shown in Eq.5, the content of bound water (m_{bw}) and unreacted calcite/vaterite (m_{CaCO_3}) of hydrated cement paste was determined using TGA. $m_s - m_{bw}$ represents the dry mass of the measured sample (i.e., sample mass m_s subtracted by m_{bw}). Thus, the fraction of unreacted $CaCO_3$ over dry mass of the measured sample can be determined. Considering the initial $CaCO_3$ content in LC^3 or VC^3 of 15%, the reacted degree of calcite/vaterite can be determined.

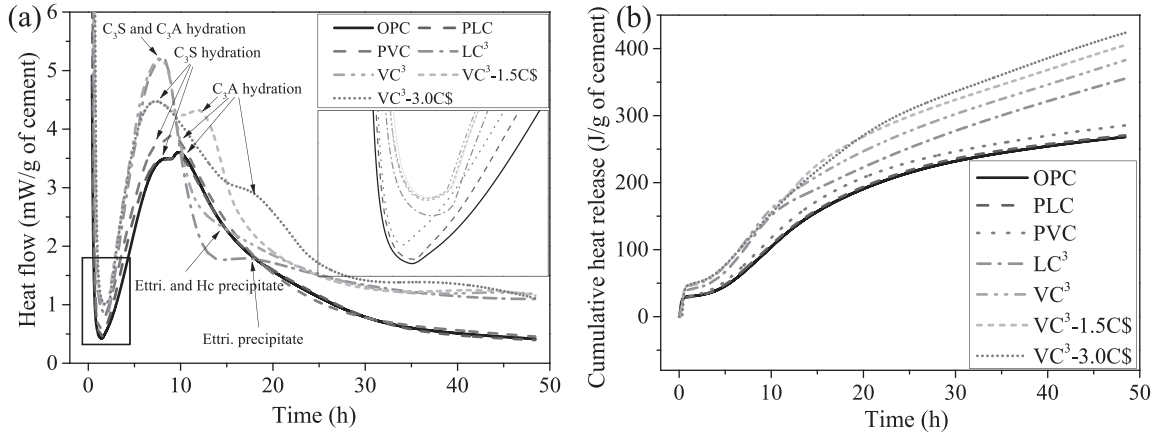

Fig. 6. Isothermal calorimetry and cumulative heat release curves of pastes of OPC, PLC, PVC, LC^3, VC^3, VC^3–1.5C$, and VC^3–3.0C$. (a) Heat flow; (b) Cumulative heat release.

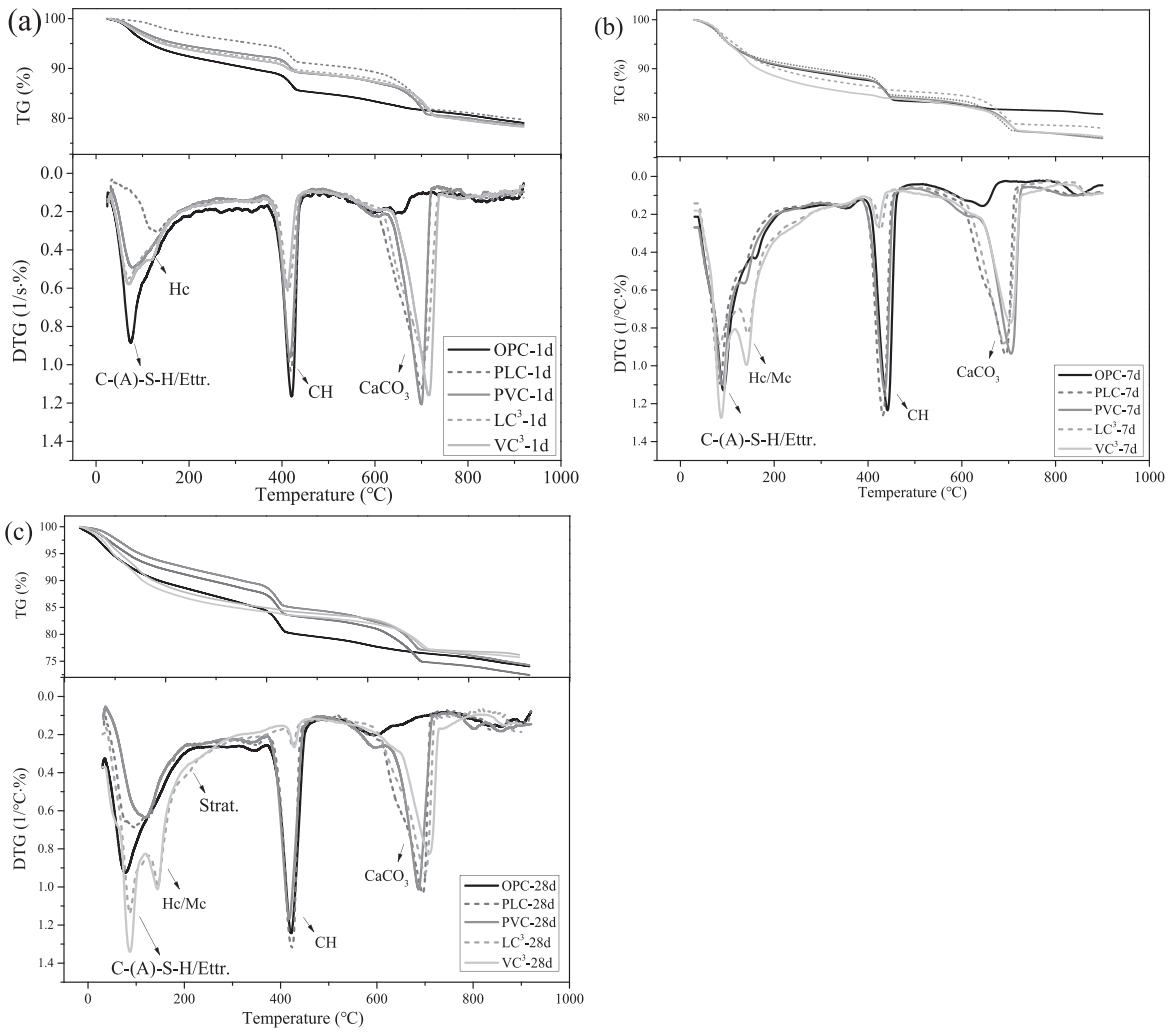

Fig. 7. Thermogravimetric analysis of pastes of OPC, PLC, PVC, LC^3, and VC^3. (a) at 1 day; (b) at 7 days; (c) at 28 days.
*Phase notation: Ettringite (Ettr.), strätlingite (Strät.), hemicarboaluminate (Hc), monocarboaluminate (Mc), portlandite (CH).

Table 4
The contents of bound water and portlandite (% of anhydrous OPC weight).

Samples	Bound water			Portlandite		
	1d	7d	28d	1d	7d	28d
OPC	14.20%	15.90%	24.33%	13.11%	18.28%	18.38%
LC^3	20.45%	30.19%	33.65%	10.90%	6.17%	1.62%
VC^3	21.51%	34.44%	35.06%	10.45%	5.83%	1.66%

$$D = 1 - \frac{m_{CaCO_3}}{m_s - m_{bw}} \Big/ 15\% \quad (5)$$

From the reaction degree of $CaCO_3$ (Table 5), calcite in LC^3 was barely consumed at 1 day, by ~11.48% at 7 days, and by ~14.53% at 28 days. Vaterite in VC^3 was consumed by 3.13 %, 21.42%, and 26.44 % at 1 day, 7 days, and 28 days, respectively. The 28-day consumption of $CaCO_3$ in LC^3 in this study is higher than the result in [10], due to the finer calcite and higher w/b used in this study. The consumption of $CaCO_3$ in VC^3 was higher than that in LC^3 as the high reactivity of vaterite led to more Mc formation in VC^3.

3.6. Pore structure

The mercury intrusion porosimetry results of LC^3 and VC^3 at 1 day are shown in Fig. 8. The total porosities of LC^3 and VC^3 were 43.3% and 48.2%, respectively (Fig. 8a).The porosity of LC^3 at 1 day is comparable to the result of [41]. The threshold pore diameters of LC^3 and VC^3 were comparable, ~830 nm (Fig. 8b). The critical pore diameters of LC^3 and VC^3 were 167 nm and 100 nm, respectively. Despite a higher total porosity of VC^3 due to the interior pores of vaterite particles [53], a

Table 5
The reaction degree of metakaolin (MK-Consumption) and $CaCO_3$ ($CaCO_3$-Consumption). The consumptions of metakaolin (MK-Consumption) are calculated from Eq.2, Eq.3 and/or Eq.4, based on the portlandite consumption (CH-Consumption) and the OPC baseline from TGA. The reaction degree of $CaCO_3$ ($CaCO_3$-Consumption) was calculated based on TGA.

Sample	CH-Consumption			MK-Consumption			$CaCO_3$-Consumption		
	1d	7d	28d	1d	7d	28d	1d	7d	28d
LC^3	16.8%	66.3%	91.2%	2.24%	11.5%	15.9%	0.31%	11.48%	14.53%
VC^3	20.3%	68.1%	91.0%	2.52%	12.4%	16.6%	3.13%	21.42%	26.44%

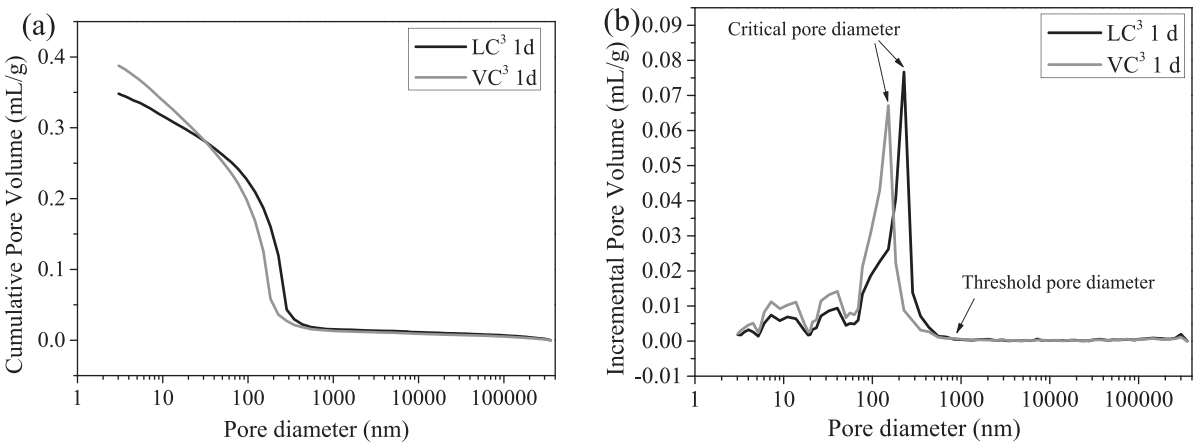

Fig. 8. Pore structures of LC^3 and VC^3 at 1 day obtained by mercury intrusion porosimetry. (a) Cumulative pore volume; (b) Incremental pore volume.

refined pore microstructure was observed in VC^3, compared to LC^3, indicating a higher hydration degree of VC^3 at 1 day, consistent with our calorimetry and thermogravimetry results. Pore size, rather than total porosity, has a more significant influence on the strength of cement-based materials [54]. The refined pore structure of VC^3 at 1 day explains the higher 1-day strength of VC^3 compared with LC^3.

3.7. Microstructures

Vaterite microspheres were wrapped by hydration products in the hardened paste of PVC and VC^3 at 1 day (Fig. 9a and Fig. 9c), while only a small part of calcite surfaces was covered by hydration products in the hardened paste of LC^3 at 1 day (Fig. 9e). EDS analysis indicates that the surface of vaterite and calcite intermixed with C-(A)-S-H gel at 1 day. At 28 days, vaterite/calcite in PVC, VC^3, and LC^3 pastes (Fig. 9b, Fig. 9d, and Fig. 9f) were all wrapped by Ca-, Al-, and Si-rich hydration products, i.e., AFm phases (Hc, Mc, and Strätlingite) and C-A-S-H gel, based on the results of EDS, XRD, and TGA. Vaterite microspheres, which were initially hollow before blending, were filled with hydration products, i.e., AFm phases (Hc and Mc) and C-(A)-S-H, at 28 days. This void filling mechanism was not observed in calcite-blended systems due to the solid nature of calcite particles. This difference indicates that pore solution can penetrate porous vaterite microspheres, forming AFm phases (Hc and Mc) and C-(A)-S-H in the interior vaterite particles, which were more densely filled in VC^3 than in PVC.

When the paste strength was low (e.g., at 1 day), the fracture occurred at the interface between vaterite/calcite and hydration products, not through $CaCO_3$ crystallites. When the paste strength was high (e.g., at 28 days), the fracture surface of PVC and VC^3 passed through vaterite crystallites. In contrast, the fracture surface of LC^3 at 28 days still appeared at the interface between calcite and hydration products. The difference may be explained that the lower density of vaterite (~2.54 g/cm^3 compared to ~2.71 g/cm^3 for calcite) and nonuniformity induced by the porous hollow structure resulted in the lower strength of vaterite.

Fig. 10 shows the Si/Ca molar ratios and Al/Ca molar ratios of C-(A)-S-H of OPC, VC^3, and LC^3. In Table 6, the Si/Ca ratios and Al/Ca ratios of C-(A)-S-H of VC^3 and LC^3 were significantly higher than those of OPC due to the pozzolanic reaction between metakaolin and portlandite. In both LC^3 and VC^3, the outer hydration products exhibited higher Si/Ca ratios and Al/Ca ratios than the inner products due to the influence of intermixing with other phases present [55]. In LC^3, the higher reaction degree of metakaolin led to higher Si/Ca ratios and Al/Ca ratios of hydration products [42]. Compared with [42,55], the Si/Ca ratios and Al/Ca ratios of LC^3 in this study are slightly higher, likely caused by the higher reaction degree of metakaolin due to the high reactivity and purity of metakaolin used in this study. The Si/Ca ratios and Al/Ca ratios of the hydration products of LC^3 and VC^3 were comparable, while the average Si/Ca ratios and Al/Ca ratios of hydration products of VC^3 were slightly higher than those of LC^3 except for the Al/Ca ratios of inner hydration products. This difference indicates that more metakaolin participated in the reaction in VC^3, consistent with our XRD and TGA results.

4. Discussions

Despite excellent mechanical properties and durability [11], LC^3 at ~50% clinker content is limited in applications due to low flowability and low 1-day compressive strength [14]. Even improved by the sulfate level adjustment, the 1-day strength of LC^3 typically still remains lower than that of OPC [10,42,56]. Alternatively, by using C-S-H seeds to accelerate the early-age hydration and to improve 1-day strength [18], the workability of LC^3 would be compromised due to C-S-H seeds-caused fast-setting [57]. Furthermore, C-S-H seeds may lower the late-age strength of cement-based materials, particularly at low water-to-binder ratios due to self-desiccation [19]. Moreover, other accelerators also have limited applications in LC^3: for example, $CaCl_2$ would trigger steel rebar corrosion [58]. As now evidenced, the low 1-day strength of LC^3 could not be easily mitigated without compromising other critical engineering properties. We emphasize the significance of VC^3 that overcomes this disadvantage of LC^3 – VC^3, without compromising late-age strength, has significantly higher 1-day strength than LC^3, suggesting the efficacy of VC^3 for practical applications, especially where early-age strength is important. For the mini slump test, no significant difference in flowability between LC^3 with VC^3 was found. The altered rheology of VC^3 is worthy of systematic studies. As the microstructure of hardened paste is refined by vaterite, the potentially improved durability of VC^3 requires validation as well. As vaterite is more reactive, the influences of varying calcined clay-$CaCO_3$ ratio deserve equally high attention.

The performance enhancement enabled by using vaterite is mainly attributed to its physical (high specific surface and nucleation sites) and chemical (high solubility and reactivity) properties. The physical effect of vaterite is evidenced by the increased hydration rate of clinker due to

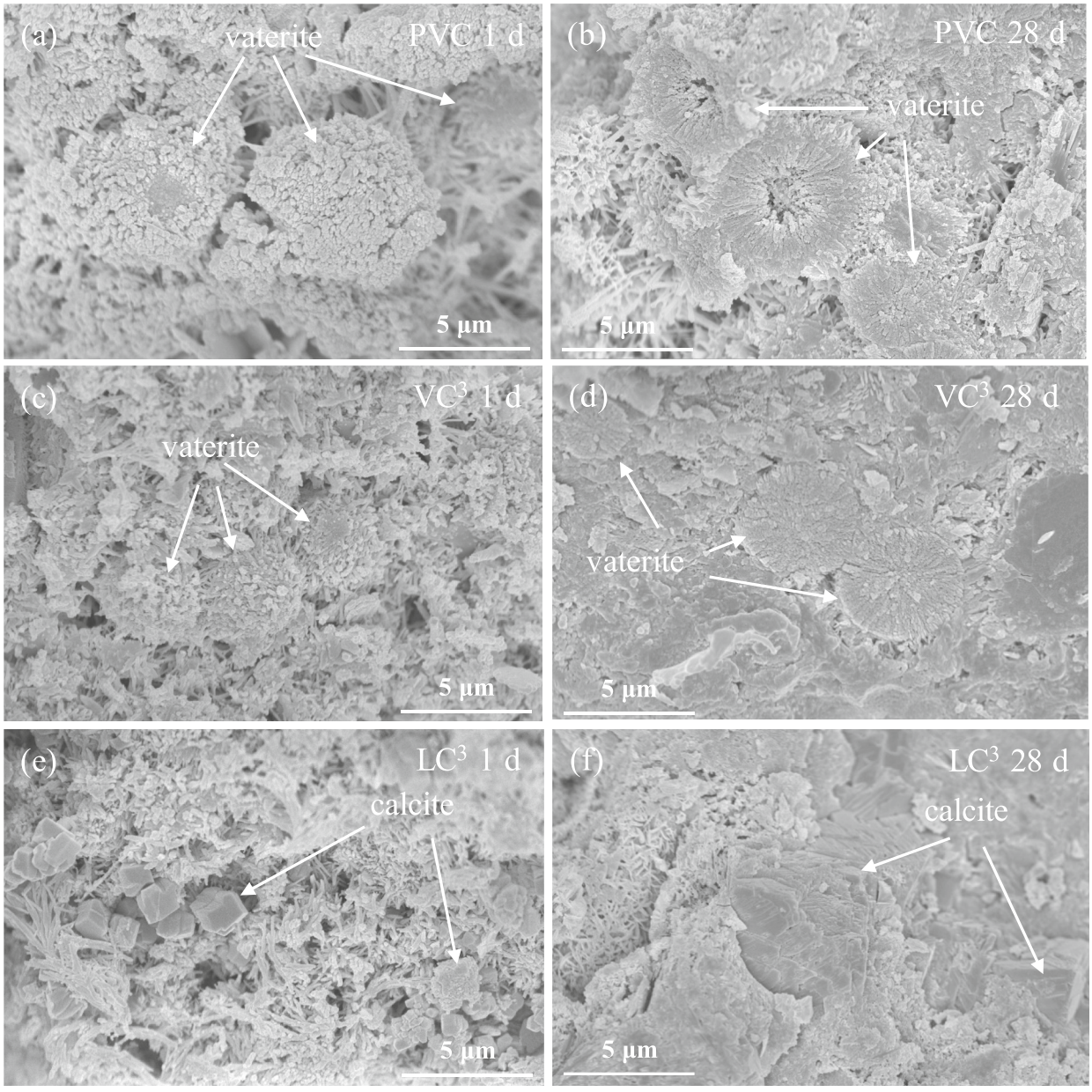

Fig. 9. SEM micrographs showing microstructures of fractured surfaces of PVC, LC^3, and VC^3 at 1 and 28 days. (a) PVC-1 day; (b) PVC-28 days; (c) VC^3–1 day; (d) VC^3–28 days; (e) LC^3–1 day; (f) LC^3–28 days.

the high specific surface area (demonstrated by the heat of hydration measurements). The chemical effect is manifested by the increased vaterite reaction degree leading to increased C-(A)-S-H formation (demonstrated with TGA) and by the increased carbonate aluminate generation (demonstrated with QXRD). In addition, the lower density of vaterite relative to calcite corresponds to a greater volume of $CaCO_3$ in VC^3 than LC^3, resulting in higher degree of $CaCO_3$ consumption in VC^3 than in LC^3. It is worth noting that VC^3 concrete requires slightly lower binder content by mass than LC^3 concrete due to the lower density of vaterite and higher strength of VC^3. As vaterite reacts faster, the VC^3 system may require lower clinker content, further reducing the embodied carbon footprint. The CO_2 emissions of calcined clay are ~400 kg/ton product [59], while the emissions of vaterite could be nearly neutral or negative depending on the sources of raw materials and manufacturing technology.

Vaterite has been widely used as a filler in chemicals or drug carriers in the biomedical industry [60,61] due to its high specific surface areas, high solubility, high dispersion, and low density [62,63]. In the construction sector [64], vaterite is used as a key phase in calcium carbonate cement [65], a promising scalable, low-carbon-footprint binder, due to the polymorph transition from vaterite to calcite and/or aragonite. However, the use of calcium carbonate cement, in civil engineering standards, is restricted from wide applications at scale. This fact jeopardizes the research and development of calcium carbonate cement and the commercialization of related entities (e.g., novel cement startups) in the field of climate/clean technology. Compared with LC^3, the VC^3

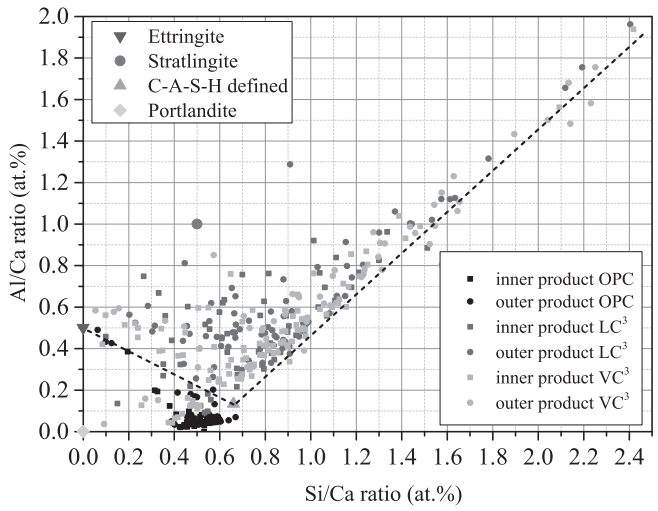

Fig. 10. Processed EDS points analysis obtained on OPC, LC^3, and VC^3 at 28 days. Al/Ca ratio is plotted as a function of Si/Ca ratio (in atomic percentage). C-A-S-H defined represents $C_{1.5}A_{0.1}SH_4$ [37].

system shows higher reactivity and early-age strength. Thus, VC^3 could potentially become a superior substitute for LC^3 for certain applications. The enhanced performance of the VC^3 cementitious system paves a way for large-scale utilization of vaterite and opens a new market for the near-term and long-term operation of the startups. The strategic utilization of vaterite in VC^3 could help the startups survive in the capital-intensive construction industry before the approval of calcium carbonate cement for broad applications by national standards and/or before the wide implementation of carbon credit.

The phase transformation of vaterite in the environment of hydrated OPC has not been reported. XRD results suggested that vaterite can stably exist in the OPC, instead of transforming into calcite or aragonite, likely due to the high alkalinity and high calcium ion content of the OPC pore solution. We examined the crystalline phase transformation of vaterite by placing it in a synthetic cement pore solution. The XRD results (Fig.s3, Supplementary Information) confirm the stable existence of vaterite in cement pore solutions. In addition, as vaterite easily transforms into calcite in high-humidity environment in the absence of high alkalinity [66], it should be stored in a sealed condition, similarly as required for cement storage. At present, vaterite can be prepared at scale by the double decomposition method and carbonization method [67–69]. The synthesis of high-purity vaterite requires precise control of the pH and reaction time in the mineralization environment or the addition of polymorph control agents [66,70], which would increase production costs. However, the high purity may be unnecessary for usage in cement/concrete because the impurity carbonates (i.e., calcite, aragonite, and dolomite) also react with Portland cement and calcined clay [32,71]. The effects of the vaterite purity on the strength development and hydration of VC^3 should be explored in the future. Moreover, the low-cost production of vaterite at the gigaton scale for the construction industry may rely on Ca-rich byproducts or wastes (e.g., mine tailing and cement kiln dust [21]). The production of vaterite by mineral carbonization can capture CO_2 directly from the air and/or point source flue gas. For 1 metric ton of $CaCO_3$ produced, 440 kg of CO_2 could be semi-permanently stored and utilized, corresponding to up to 100 kg of CO_2 stored in 1 metric ton of VC^3 cement at 1:1 calcined clay-vaterite ratio and 50% clinker content.

5. Conclusions

We developed and demonstrated a new ternary blended cement system, vaterite calcined clay cement, VC^3. 45% of ordinary Portland cement was replaced by metakaolin and metastable $CaCO_3$ polymorph vaterite at a 2:1 blend. Compared to limestone calcined clay cement, LC^3, with a similar particle size distribution, VC^3 exhibited slightly improved flowability and greatly improved compressive strengths at all ages. With 3% gypsum adjustment, VC^3 presents a 13% higher strength relative to ordinary Portland cement reference even at 1 day. The outperformance of VC^3 relative to LC^3 is explained by the metastability and thus higher reactivity of vaterite relative to calcite. Setting time and heat release measurements demonstrated the faster reaction of vaterite in VC^3 than limestone (i.e., calcite) in LC^3. XRD results showed that vaterite reacts with metakaolin, forming more hemi- and monocarboaluminate but less strätlingite than in LC^3. TGA results suggested that the formation of AFm phases and pozzolanic reaction largely consumed portlandite. Morphological studies demonstrated that the microstructure of VC^3 was refined in the presence of vaterite relative to LC^3, where hollow vaterite resulted in higher bulk porosity of VC^3 and interior filling with hydration products.

Thanks to recent advances in technologies of carbon capture, storage, and utilization (CCUS, also known as clean/climate technologies), vaterite can be massively produced (potentially 100s Mt/year) through carbon mineralization with carbon permanently stored at low costs. Besides vaterite-based cement (e.g., Fortera and Calera), vaterite can be blended to produce VC^3 for broader applications. The VC^3 system presents a reliable, high-performance complementary product to LC^3, particularly when high early-age strengths are required and/or where the LC^3 productivity is limited by limestone grinding. Therefore, VC^3 shows great promises as an enabler of CCUS technologies to mitigate climate change at scale.

CRediT authorship contribution statement

Yaqiang Li: Methodology, Investigation, Visualization, Writing – original draft, Funding acquisition. **Yue Li:** Methodology, Conceptualization, Writing – review & editing. **Hongyan Ma:** Methodology, Conceptualization, Writing – review & editing. **Jiaqi Li:** Conceptualization, Methodology, Investigation, Validation, Visualization, Writing – original draft, Funding acquisition.

Declaration of competing interest

The authors declare that they have no known competing financial interests or personal relationships that could have appeared to influence the work reported in this paper.

Data availability

Data will be made available on request.

Table 6
Average composition of C-(A)-S-H of OPC, LC^3, and VC^3 at 28 days.

Molar ratio	OPC		LC^3		VC^3	
	Inner product	Outer product	Inner product	Outer product	Inner product	Outer product
Average Si/Ca	0.482	0.505	0.755	0.958	0.791	1.08
Average Al/Ca	0.060	0.107	0.503	0.685	0.482	0.757

Acknowledgement

This work was performed under the Fundamental Research Funds for the Central Universities (grant number BLX202006) and the auspices of the U.S. Department of Energy by Lawrence Livermore National Laboratory (contract No. DEAC52-07NA27344). IM release number: LLNL-JRNL-849052.

Appendix A. Supplementary data

Supplementary data to this article can be found online at https://doi.org/10.1016/j.cemconres.2023.107374.

References

[1] S.A. Miller, V.M. John, S.A. Pacca, A. Horvath, Carbon dioxide reduction potential in the global cement industry by 2050, Cem. Concr. Res. 114 (2018) 115–124.
[2] P. Monteiro, S.A. Miller, A. Horvath, Towards sustainable concrete, Nat. Mater. 16 (7) (2017) 698–699.
[3] E. Gartner, Industrially interesting approaches to "low-CO2" cements, Cem. Concr. Res. 34 (9) (2004) 1489–1498.
[4] S.A. Miller, R.J. Myers, Environmental impacts of alternative cement binders, Environ. Sci. Technol. 54 (2) (2020) 677–686.
[5] R. Snellings, G. Mertens, J. Elsen, Supplementary cementitious materials, Applied Mineralolgy of Cement & Concrete 74 (2012) 211–278.
[6] M.C.G. Juenger, R. Snellings, S.A. Bernal, Supplementary cementitious materials: new sources, characterization, and performance insights, Cem. Concr. Res. 122 (2019) 257–273.
[7] K. Scrivener, F. Martirena, S. Bishnoi, S. Maity, Calcined clay limestone cements (LC3), Cem. Concr. Res. 114 (2018) 49–56.
[8] F. Zunino, F. Martirena, K. Scrivener, Limestone calcined clay cements (LC3), ACI materials journal 4 (2021) 118.
[9] K. Scrivener, F. Avet, H. Maraghechi, F. Zunino, J. Ston, W. Hanpongpun, A. Favier, Impacting factors and properties of limestone calcined clay cements (LC3), GREEN MATERIALS 7 (1) (2019) 3–14.
[10] M. Antoni, J. Rossen, F. Martirena, K. Scrivener, Cement substitution by a combination of metakaolin and limestone, Cem. Concr. Res. 42 (12) (2012) 1579–1589.
[11] Y. Dhandapani, T. Sakthivel, M. Santhanam, R. Gettu, R.G. Pillai, Mechanical properties and durability performance of concretes with limestone calcined clay cement (LC3), Cem. Concr. Res. 107 (2018) 136–151.
[12] M. Sharma, S. Bishnoi, F. Martirena, K. Scrivener, Limestone calcined clay cement and concrete: a state-of-the-art review, Cem. Concr. Res. 149 (2021), 106564.
[13] S. Krishnan, A.C. Emmanuel, V. Shah, A. Parashar, S. Bishnoi, Industrial production of limestone calcined clay cement (LC 3) – experience and insights, Green Materials 7 (1) (2018) 15–27.
[14] R. Hay, L. Li, K. Celik, Shrinkage, hydration, and strength development of limestone calcined clay cement (LC3) with different sulfation levels, Cement and Concrete Composites 127 (2022), 104403.
[15] O. Canbek, Q. Xu, Y. Mei, N.R. Washburn, K.E. Kurtis, Predicting the rheology of limestone calcined clay cements (LC3): linking composition and hydration kinetics to yield stress through machine learning, Cem. Concr. Res. 160 (2022), 106925.
[16] USGS, Mineral Commodity Summaries 2019, Government Printing Office, 2019.
[17] P.K. Mehta, P.J. Monteiro, Concrete Microstructure, Properties and Materials, McGraw-Hill, New York, 2017.
[18] J. Li, W. Zhang, K. Xu, P.J.M. Monteiro, Fibrillar calcium silicate hydrate seeds from hydrated tricalcium silicate lower cement demand, Cem. Concr. Res. 137 (2020), 106195.
[19] M. Wyrzykowski, A. Assmann, C. Hesse, P. Lura, Microstructure development and autogenous shrinkage of mortars with C-S-H seeding and internal curing, Cem. Concr. Res. 129 (2020), 105967.
[20] C.W. Hargis, A. Telesca, P.J.M. Monteiro, Calcium sulfoaluminate (Ye'elimite) hydration in the presence of gypsum, calcite, and vaterite, Cem. Concr. Res. 65 (2014) 15–20.
[21] C.W. Hargis, I.A. Chen, M. Devenney, M.J. Fernandez, R.J. Gilliam, R.P. Thatcher, Calcium carbonate cement: a carbon capture, utilization, and storage (CCUS) technique, Materials 14 (11) (2021) 2709.
[22] Y. Mori, T. Enomae, A. Isogai, Preparation of pure vaterite by simple mechanical mixing of two aqueous salt solutions, Mater. Sci. Eng. C 29 (4) (2009) 1409–1414.
[23] Q. Shen, H. Wei, Y. Zhou, Y. Huang, H. Yang, D. Wang, D. Xu, Properties of amorphous calcium carbonate and the template action of Vaterite spheres, J. Phys. Chem. B. 110 (7) (2006) 2994–3000.
[24] Z. Tan, S.A. Bernal, J.L. Provis, Reproducible mini-slump test procedure for measuring the yield stress of cementitious pastes, Mater. Struct. 50 (6) (2017) 235.
[25] B.G. Kutchko, A.G. Kim, Fly ash characterization by SEM–EDS, Fuel 85 (17) (2006) 2537–2544.
[26] T.R. Muzenda, P. Hou, S. Kawashima, T. Sui, X. Cheng, The role of limestone and calcined clay on the rheological properties of LC3, Cement and Concrete Composites 107 (2020), 103516.
[27] E. Berodier, K. Scrivener, Understanding the filler effect on the nucleation and growth of C-S-H, J. Am. Ceram. Soc. 97 (12) (2014) 3764–3773.
[28] T. Matschei, B. Lothenbach, P.F. Glasser, The role of calcium carbonate in cement hydration, Cem. Concr. Res. 37 (4) (2007) 551–558.
[29] Y. Briki, M. Zajac, M.B. Haha, K. Scrivener, Impact of limestone fineness on cement hydration at early age, Cem. Concr. Res. 147 (2021), 106515.
[30] D. Lootens, P. Jousset, L. Martinie, N. Roussel, R.J. Flatt, Yield stress during setting of cement pastes from penetration tests, Cem. Concr. Res. 39 (5) (2009) 401–408.
[31] S.E. Schulze, J. Rickert, Suitability of natural calcined clays as supplementary cementitious material, Cement and Concrete Composites 95 (2019) 92–97.
[32] S. Krishnan, S. Bishnoi, Understanding the hydration of dolomite in cementitious systems with reactive aluminosilicates such as calcined clay, Cem. Concr. Res. 108 (2018) 116–128.
[33] A.D. Visscher, J. Vanderdeelen, Estimation of the solubility constant of calcite, aragonite, and Vaterite at 25°C based on primary data using the Pitzer ion interaction approach, Monatshefte Fur Chemie 134 (2003) 769–775.
[34] H. Huang, X. Li, F. Avet, W. Hanpongpun, K. Scrivener, Strength-promoting mechanism of alkanolamines on limestone-calcined clay cement and the role of sulfate, Cem. Concr. Res. 147 (2021), 106527.
[35] M. Zajac, A. Rossberg, G. Le Saout, B. Lothenbach, Influence of limestone and anhydrite on the hydration of Portland cements, Cement and Concrete Composites 46 (2014) 99–108.
[36] F. Georget, B. Lothenbach, W. Wilson, F. Zunino, K.L. Scrivener, Stability of hemicarbonate under cement paste-like conditions, Cem. Concr. Res. 153 (2022), 106692.
[37] F. Zunino, Y. Dhandapani, M. Ben Haha, J. Skibsted, S. Joseph, S. Krishnan, A. Parashar, M.C.G. Juenger, T. Hanein, S.A. Bernal, K.L. Scrivener, F. Avet, Hydration and mixture design of calcined clay blended cements: review by the RILEM TC 282-CCL, Materials and Structures 55 (9) (2022) 234.
[38] A. Tironi, M.A. Trezza, A.N. Scian, E.F. Irassar, Thermal analysis to assess pozzolanic activity of calcined kaolinitic clays, J. Therm. Anal. Calorim. 117 (2) (2014) 547–556.
[39] M. Maier, S. Scherb, A. Neißer-Deiters, N. Beuntner, K.-C. Thienel, Hydration of cubic tricalcium aluminate in the presence of calcined clays, J. Am. Ceram. Soc. 104 (7) (2021) 3619–3631.
[40] Maciej Zajac, Anne Rossberg, Gwenn Le Saout, Barbara Lothenbach, Influence of limestone and anhydrite on the hydration of Portland cements, Cement and Concrete Composites 46 (2014) 99–108.
[41] F. Zunino, K. Scrivener, The reaction between metakaolin and limestone and its effect in porosity refinement and mechanical properties, Cem. Concr. Res. 140 (2021), 106307.
[42] F. Avet, K. Scrivener, Investigation of the calcined kaolinite content on the hydration of limestone calcined clay cement (LC3), Cem. Concr. Res. 107 (2018) 124–135.
[43] M.U. Okoronkwo, F.P. Glasser, Stratlingite: compatibility with sulfate and carbonate cement phases, MATERIALS AND STRUCTURES 49 (9) (2016) 3569–3577.
[44] M.U. Okoronkwo, F.P. Glasser, Stability of stratlingite in the CASH system, Mater. Struct. 49 (10) (2016) 4305–4318.
[45] M.U. Okoronkwo, F.P. Glasser, Compatibility of hydrogarnet, Ca3Al2(SiO4)(x)(OH)(4(3-x)), with sulfate and carbonate-bearing cement phases: 5-85 degrees C, Cem. Concr. Res. 83 (2016) 86–96.
[46] B. Lothenbach, K. Scrivener, R.D. Hooton, Supplementary cementitious materials, Cem. Concr. Res. 41 (12) (2011) 1244–1256.
[47] D. Marchon, P. Juilland, E. Gallucci, L. Frunz, R.J. Flatt, Molecular and submolecular scale effects of comb-copolymers on tri-calcium silicate reactivity: toward molecular design, J. Am. Ceram. Soc. 100 (3) (2017) 817–841.
[48] M. Maier, R. Sposito, N. Beuntner, K.-C. Thienel, Particle characteristics of calcined clays and limestone and their impact on early hydration and sulfate demand of blended cement, Cem. Concr. Res. 154 (2022), 106736.
[49] X. Chen, X. Yang, K. Wu, Q. Chen, Z. Yang, L. Xu, H. Li, Understanding the role of C–S–H seed/PCE nanocomposites, triethanolamine, sodium nitrate and PCE on hydration and performance at early age, Cement and Concrete Composites 139 (2023), 105002.
[50] A. Dixit, H. Du, J. Dang, S.D. Pang, Quaternary blended limestone-calcined clay cement concrete incorporating fly ash, Cement and Concrete Composites 123 (2021), 104174.
[51] K. De Weerdt, M.B. Haha, G. Le Saout, K.O. Kjellsen, H. Justnes, B. Lothenbach, Hydration mechanisms of ternary Portland cements containing limestone powder and fly ash, Cem. Concr. Res. 41 (3) (2011) 279–291.
[52] B.K. Marsh, R.L. Day, Pozzolanic and cementitious reactions of fly ash in blended cement pastes, Cem. Concr. Res. 18 (2) (1988) 301–310.
[53] T. Beuvier, B. Calvignac, G.J.-R. Delcroix, M.K. Tran, S. Kodjikian, N. Delorme, J.-F. Bardeau, A. Gibaud, F. Boury, Synthesis of hollow vaterite CaCO3 microspheres in supercritical carbon dioxide medium, J. Mater. Chem. 21 (2011) 9757–9761.
[54] Y. Dhandapani, M. Santhanam, Assessment of pore structure evolution in the limestone calcined clay cementitious system and its implications for performance, Cem. Concr. Compos. 84 (2017) 36–47.
[55] F. Avet, X. Li, K. Scrivener, Determination of the amount of reacted metakaolin in calcined clay blends, Cem. Concr. Res. 106 (2018) 40–48.
[56] O. Akhlaghi, T. Aytas, B. Tatli, D. Sezer, A. Hodaei, A. Favier, K. Scrivener, Y. Z. Menceloglu, O. Akbulut, Modified poly(carboxylate ether)-based superplasticizer for enhanced flowability of calcined clay-limestone-gypsum blended Portland cement, Cem. Concr. Res. 101 (2017) 114–122.
[57] C. Bhojaraju, M. Charrier, C.M. Ouellet-Plamondon, How admixtures affect yield stresses of cement, ACI Mater. J. 6 (2021) 118.

[58] A. Poursaee, A. Laurent, C.M. Hansson, Corrosion of steel bars in OPC mortar exposed to NaCl, MgCl2 and CaCl2: macro- and micro-cell corrosion perspective, Cem. Concr. Res. 40 (3) (2010) 426–430.
[59] Y. Cancio Díaz, S. Sánchez Berriel, U. Heierli, A.R. Favier, I.R. Sánchez Machado, K. L. Scrivener, J.F. Martirena Hernández, G. Habert, Limestone calcined clay cement as a low-carbon solution to meet expanding cement demand in emerging economies, development, Engineering 2 (2017) 82–91.
[60] D.B. Trushina, T.V. Bukreeva, M.V. Kovalchuk, M.N. Antipina, CaCO3 vaterite microparticles for biomedical and personal care applications, Mater. Sci. Eng. C 45 (2014) 644–658.
[61] L.-H. Fu, C. Qi, Y.-R. Hu, C.-G. Mei, M.-G. Ma, Cellulose/vaterite nanocomposites: Sonochemical synthesis, characterization, and their application in protein adsorption, Mater. Sci. Eng. C 96 (2019) 426–435.
[62] W. Li, C. Gao, Efficiently stabilized spherical Vaterite CaCO3 crystals by carbon nanotubes in biomimetic mineralization, Langmuir 23 (8) (2007) 4575–4582.
[63] J. Feng, G. Wu, C. Qing, Biomimetic synthesis of hollow calcium carbonate with the existence of the agar matrix and bovine serum albumin, Materials Science Engineering C 58 (2016) 409–411.
[64] O. Cherkas, T. Beuvier, F. Zontone, Y. Chushkin, L. Demoulin, A. Rousseau, A. Gibaud, On the kinetics of phase transformations of dried porous vaterite particles immersed in deionized and tap water, Adv. Powder Technol. 29 (11) (2018) 2872–2880.
[65] P.J.M. Monteiro, L. Clodic, F. Battocchio, W. Kanitpanyacharoen, S.R. Chae, J. Ha, H.-R. Wenk, Incorporating carbon sequestration materials in civil infrastructure: a micro and nano-structural analysis, Cement and Concrete Composites 40 (2013) 14–20.
[66] R. Ševčík, M. Pérez-Estébanez, A. Viani, P. Šašek, P. Mácová, Characterization of vaterite synthesized at various temperatures and stirring velocities without use of additives, Powder Technol. 284 (2015) 265–271.
[67] D. Konopacka-Łyskawa, Synthesis methods and favorable conditions for spherical vaterite precipitation: a review, Crystals 9 (4) (2019) 223.
[68] S. Kim, J. Jeon, M.-J. Kim, Vaterite production and particle size and shape control using seawater as an indirect carbonation solvent, J. Environ. Chem. Eng. 10 (2) (2022), 107296.
[69] X. Liu, B. Wang, Z. Zhang, Z. Pan, H. Cheng, F. Cheng, Glycine-induced synthesis of vaterite by direct aqueous mineral carbonation of desulfurization gypsum, Environ. Chem. Lett. 20 (4) (2022) 2261–2269.
[70] Y. Sheng Han, G. Hadiko, M. Fuji, M. Takahashi, Crystallization and transformation of vaterite at controlled pH, J. Cryst. Growth 289 (1) (2006) 269–274.
[71] Y. Dhandapani, M. Santhanam, G. Kaladharan, S. Ramanathan, Towards ternary binders involving limestone additions — a review, Cem. Concr. Res. 143 (2021), 106396.